RSC Advances

PAPER

View Article Online
View Journal | View Issue

Cite this: *RSC Adv.*, 2025, **15**, 15490

Black palladium nanoparticle-based lateral flow immunoassay for cardiovascular disease diagnosis†

Hong Ding,‡[a] Yao Nie,‡[b] Zhen Chen,‡[a] Wanchao Zuo,[b] Juan Cao,[a] Zihan Ling,[c] Yanmin Ju *[b] and Ming Chen*[d]

Lateral flow immunoassay (LFIA) based on gold nanoparticles (AuNPs) has emerged as a rapid and cost-effective tool for point-of-care diagnostics, yet it remains limited by its low sensitivity in colorimetric detection. Herein, we report a black palladium nanoparticle (PdNP)-based LFIA system for the detection of lipoprotein-associated phospholipase A2 (Lp-PLA2), a key biomarker of cardiovascular diseases. The intrinsic black color of PdNPs provided higher visual discriminability at low concentrations compared with AuNPs. Moreover, PdNP probes synthesized through chemical covalent conjugation with antibodies had the advantages of enhancing the target recognition ability. The PdNP-based LFIA achieved a 12-fold lower visual detection limit and a 100-fold wider linear range compared with AuNP-based LFIA. Moreover, clinical validation detection results using 57 serum samples were in strong accordance with the clinical methods. This work not only establishes PdNP-based LFIA to address the long-standing sensitivity limitations of colorimetric LFIA, but also offers a robust diagnostic tool for early cardiovascular disease diagnosis in resource-limited settings.

Received 1st April 2025
Accepted 24th April 2025

DOI: 10.1039/d5ra02274f

rsc.li/rsc-advances

1. Introduction

Lateral flow immunoassay (LFIA) is a solid-phase membrane immunoassay that integrates immunotechnology and chromatography.[1–3] Characterized by low cost, simplicity, and ease of operation, it can directly confirm the presence of target analytes without the need for a laboratory environment.[4–6] Nowadays, it has been extensively applied in fields such as medical diagnosis,[7] ecological monitoring,[8] and agricultural monitoring.[9] Among them, gold nanoparticle (AuNP) immunochromatography is the most common system. It can be assessed in real time through naked-eye colorimetry, eliminating the need for laboratory equipment and professional operations, thus being convenient to use.[10–13] However, owing to the relatively weak colorimetric signal intensity of AuNPs, it currently faces the challenge of insufficient detection sensitivity. Therefore, developing a highly sensitive colorimetric signal strategy is of great practical significance for LFIA. This not only ensures the convenience of visual signal reading but also provides a reliable basis for the application of LFIA in the analysis of trace targets.

Currently, most of the proposed colorimetric signal-based LFIA detection methods such as enzyme catalysis,[14–16] nanoparticle aggregation,[10,17–19] and chemiluminescence-colorimetry conversion[20–23] require additional steps to enhance the detection signal. Moreover, these amplification strategies are achieved using additional signal enhancement reagents, which not only need to strictly ensure the storage stability and safety of enhancement reagents, but also increase the workload and the detection time.[24–26] Another way to improve the sensitivity of LFIA is to change the nanoparticles used for LFIA labeling, thereby lowering the detection limit. The properties of nanoparticles largely determine their optical characteristics, which, in turn, determine the minimum number of nanoparticles required to detect the target on test strips.[27] Recently, a research study compared the differences in detection performance when red gold nanoparticles, black gold@platinum nanoparticles, green latex nanoparticles, and brown magnetic nanoparticles were applied as labels in LFIA, and the results indicated that black labels may be the most effective color markers on test strips.[28] In addition, the molar extinction coefficient inherent in noble metal-based nanoparticles has an important effect on their optical properties such as optical density. In general, darker materials have higher molar extinction coefficients and are easier to distinguish with the naked eye. Theoretically, noble metal nanoparticles with black color are expected to be used as excellent labels for LFIA to achieve signal sensitization.

[a]*Department of Cardiology, Taixing People's Hospital, Taixing, Jiangsu, 225400, China. E-mail: 511978653@qq.com; zhench_cn@163.com; 1016526899@qq.com*

[b]*College of Pharmacy, China Pharmaceutical University, Nanjing, Jiangsu, 211198, China. E-mail: 1562037162@qq.com; Affection9797616@163.com; juyanmin@cpu.edu.cn*

[c]*North Sichuan Medical College, No. 55 Dongshun Road, Nanchong, Sichuan, 637000, China. E-mail: 2945271623@qq.com*

[d]*Department of Clinical Laboratory Taixing People's Hospital, The Sixth Affiliated Hospital of Yangzhou University, Taixing, Jiangsu, 225400, China. E-mail: Chenmingbox@hotmail.com*

† Electronic supplementary information (ESI) available. See DOI: https://doi.org/10.1039/d5ra02274f

‡ Both authors contributed equally to this work.

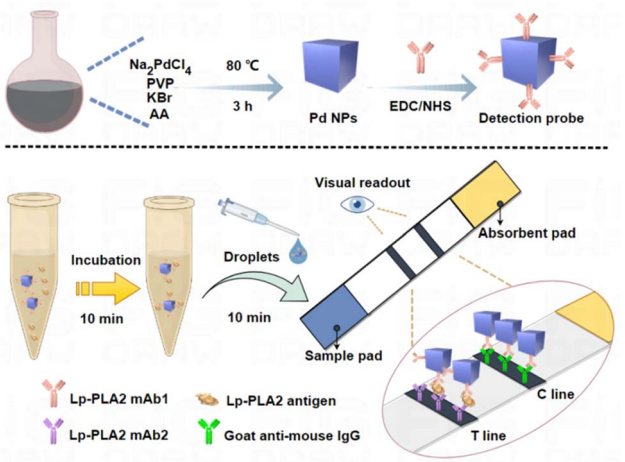

Scheme 1 Synthesis of PdNP detection probes and illustration of PdNP-based LFIA biosensors.

Herein, black nanotag palladium nanoparticles (PdNPs) based on the molar extinction coefficient effect are proposed to be applied to LFIA test strips for the detection of lipoprotein-associated phospholipaseA2 (Lp-PLA2) (Scheme 1), one of the indications of cardiovascular diseases.[29–31] First, PdNPs with a size of about 18 nm were successfully synthesized, the nanoparticles showed good stability. When compared with the AuNP's color (the same size with PdNPs), the same concentration of PdNPs showed more obvious and distinguishable colors. Interestingly, PdNP probes synthesized *via* chemical covalent conjugation with antibodies had the advantages of enhancing the target recognition ability. There was further optimization of detection conditions, and the sensitivity can be improved 12-fold to 5 ng mL^{-1} compared with AuNPs under optimized conditions. We clinically tested 57 serum samples and found that the results were basically consistent with the clinical detection results, with an receiver operating characteristic curve (ROC) value of 0.98. Therefore, the application of black PdNPs as labels for LFIA can achieve high sensitively detection without relying on the addition of additional reagents, which provides an informative new idea for achieving LFIA easy to use.

2. Materials and methods

2.1 Materials

Unless otherwise explicitly stated, all reagents used in this study were of analytical reagent grade or possessed a higher quality level. Sodium tetrachloropalladate(II) (Na_2PdCl_4), potassium bromide (KBr), bovine serum albumin (BSA), and chloroauric acid trihydrate ($HAuCl_4 \cdot 3H_2O$) were purchased from Aladdin (Shanghai, China). 1-(3-Dimethylaminopropyl)-3-ethylcarbodiimide hydrochloride (EDC), *N*-hydroxysuccinimide (NHS), polyvinyl pyrrolidone (PVP), L-ascorbic acid (AA), thioglycolic acid, and casein sodium were acquired from Macklin (Shanghai, China). The lipoprotein-associated phospholipaseA2 (Lp-PLA2) protein and Anti-Lp-PLA2 monoclonal antibodies (mAb1 and mAb2) were provided by Bioantibody Biotechnology Co. Ltd (Nanjing, China). Goat anti-mouse IgG was purchased from Jackson ImmunoResearch Inc. Nitrocellulose (NC) membranes were obtained from Sartorius Corporation. Polyester sample pads, polyvinyl chloride (PVC) backboard, and absorbent pads were sourced from Hangzhou Autokun Technology.

2.2 Characterization

TEM images were acquired by transmission electron microscopy (FEI Tecnai T20), and the software Nano Measurer was used to measure the size of PdNPs in TEM. X-ray diffraction (XRD) measurements were conducted using a powder X-ray diffraction system (D/max-2400) equipped with a Cu Kα radiation source of wavelength 1.54 Å. X-ray photoelectron spectroscopy (XPS) data were obtained using a PerkinElmer PHI 5600 instrument. The hydrodynamic diameter was measured using a BeNano 90 Nano Particle Size Analyzer.

2.3 Synthesis of PdNPs

The round-bottom flask was preheated in an oil bath at 80 °C for 10 min. Subsequently, 105 mg PVP, 60 mg AA, and 600 mg KBr were added into 8 mL deionized water. The resulting mixture was dissolved by ultrasonication and then transferred into a preheated round-bottom flask continuously stirred at 80 °C for 10 min. Subsequently, 3 mL aqueous solution of 19 mg mL^{-1} Na_2PdCl_4 was added to the reaction mixture. The reaction was allowed to proceed at 80 °C for 3 h and then gradually cooled to room temperature. Subsequently, the mixture was centrifuged at 50 000*g* for 10 min. The collected precipitate was washed twice with deionized water and resuspended in 5 mL of deionized water. The obtained suspension was stored at 4 °C for later use.

2.4 Synthesis of AuNPs

First, 100 mL deionized water was transferred into an appropriate reaction vessel. Subsequently, water was heated to boiling under continuous magnetic stirring. Immediately after reaching the boiling point, 1 mL 1% (w/v) $HAuCl_4 \cdot 3H_2O$ solution was introduced into the boiling water, and the mixture was vigorously stirred for 2 min. Thereafter, 4 mL 1% (w/v) sodium citrate solution was added to the reaction system. The boiling process was maintained until a distinct color transition to wine red was observed in the solution. Subsequently, the solution was continuously stirred for 20 min, allowed to cool naturally to room temperature and then stored at 4 °C for later use.

2.5 Conjugation of PdNPs and AuNPs with antibodies

The conjugation of PdNPs with antibodies was accomplished *via* the EDC/NHS-mediated covalent chemical conjugation method.[32–34] In the initial step, PdNPs were incubated with thioglycolic acid for 12 h. This incubation led to the formation of PdNPs-COOH. Subsequently, the product was centrifuged at 12 000 rpm for 10 min and then resuspended in phosphate buffer (PB) (0.01 M, pH 6.0). Subsequently, 50 μL 20 mM EDC and 50 μL 50 mM NHS were added to the solution, followed by

the addition of 15 μL 1 mg mL^{-1} Lp-PLA2 mAb1. The mixture was allowed to react continuously for 4 h. Thereafter, 100 μL 10% (w/v) BSA was introduced to block the unbound sites on the surface of PdNPs for 1 h, thereby preventing non-specific binding. The mixture was then centrifuged at 12 000 rpm, washed twice with water, and finally resuspended in a storage buffer composed of 1% (w/v) BSA and 10% (w/v) sucrose for subsequent applications.

For the preparation of AuNP probes, the pH of 1 mL AuNP solution was adjusted to 8–9 using 0.1 M K_2CO_3. Subsequently, 15 μL 1 mg mL^{-1} Lp-PLA2 mAb1 was added to the pH-adjusted AuNP solution. The mixture was then subjected to gentle rotation for 1 h. After that, 100 μL 10% (w/v) BSA was added to the reaction mixture to block the unbound sites for 30 min. Subsequently, the mixture was centrifuged at 15 000 rpm for 10 min and washed once with water, and the resulting product was resuspended in 200 μL of storage buffer containing 1% (w/v) BSA and 10% (w/v) sucrose.

2.6 Fabrication of LFIA test strips

The fabrication process of the test strips involved the integration of four essential components: sample pad, NC membrane, PVC backboard, and absorbent pad. These components were meticulously assembled onto the PVC backboard, ensuring an overlap of 2 mm between adjacent parts. Subsequently, Lp-PLA2 mAb2 with a concentration of 1 mg mL^{-1} was precisely dispensed onto the NC membrane at a dispensing rate of 1 μL cm^{-1}, thereby forming the test line. Meanwhile, goat anti-mouse IgG (1 mg mL^{-1}) was dispensed using the identical spraying process to establish the control line. The assembled board was then placed within an oven pre-set at 37 °C and left to dry for 2 h. Then the board was cut into individual test strips, each having a width of 3 mm, ready for further analyses.

2.7 Detection of Lp-PLA2 using LFIA strips

For the evaluation of the detection proficiency of the test strips, the detection solutions were first mixed with the pre-synthesized probes for a duration of 10 min. Subsequently, 1% casein–sodium blocking solution containing 0.01% Tween 20 was added. Thereafter, the resulting mixture was carefully added dropwise onto the sample pad of the test strips. Under the influence of capillary action, the liquid migrated across the NC membrane. Once all the mixture had reached the absorbent pad, a discernible black band was formed at both the test line and the control line. For the quantification of the bands, the 'COLOR PICKER' software was employed to read the RGB values. Regarding the detection and quantification of the AuNPs test strips, the approach was consistent with the aforementioned procedure.

2.8 Testing of clinical samples using LFIA strips

The human serum samples were kindly provided by Taixing People's Hospital (LS2025023). First, these serum samples were diluted three times with PBS. Subsequently, the diluted serum samples were incubated with the previously prepared probes for 10 min. After that, the blocking solution was added to the mixture. Next, the resulting mixture solution was carefully dropped onto the test strips for the purpose of detection. It should be noted that each sample was repeatedly detected three times under identical conditions. Finally, the obtained results were analyzed by employing the above-described method, ensuring the reliability and reproducibility of the experimental data.

3. Results

3.1 Synthesis and characterization of PdNPs

A series of characterizations were carried out to verify the synthesized PdNPs. Transmission electron microscopy (TEM) results revealed that PdNPs were highly dispersed and exhibited a tetrahedral morphology with a length of 17.90 ± 1.46 nm (Fig. 1a–c). The X-ray diffraction (XRD) patterns of PdNPs (Fig. 1d) were in good agreement with the standard spectra (PDF #46-1043). The high-resolution XPS spectrum indicated that the main components of PdNPs were Pd, C, N, and O (Fig. S1†). Specifically, PdNPs consisted of metallic Pd (Pd^0: $3d_{5/2}$, 334.7 eV; $3d_{3/2}$, 340.3 eV) and a small amount of oxidized Pd (Pd^{2+}: $3d_{5/2}$, 337.3 eV; $3d_{3/2}$, 342.9 eV) (Fig. 1e). These findings confirmed the successful synthesis of PdNPs.

Notably, after 90 days of storage, the physical properties of the synthesized PdNPs remained unaltered, demonstrating excellent stability (Fig. 1f). Interestingly, while the PdNPs and AuNPs exhibited comparable sizes (Fig. S2a and b†), PdNPs demonstrated a significantly enhanced colorimetric signal at equivalent concentrations. A side-by-side comparison of color visibility across a concentration gradient (6.25–1000 ng mL^{-1}) revealed that AuNP signals became indistinguishable to the naked eye at 25 ng mL^{-1}, whereas PdNPs retained clear visual resolution even at 6.25 ng mL^{-1} (Fig. S3†), and the enhanced visual resolution of PdNPs can be attributed to their strong light absorption in the visible spectrum. As black materials exhibit a higher optical density than AuNPs under ambient conditions, it is suggested that PdNPs show potential as a colorimetric probe. Subsequently, PdNPs were conjugated with Lp-PLA2 mAb1 through chemical covalent to explore their feasibility as detection probes; at the same time, the AuNPs and antibody coupling were also compared as a control, and a hydrodynamic

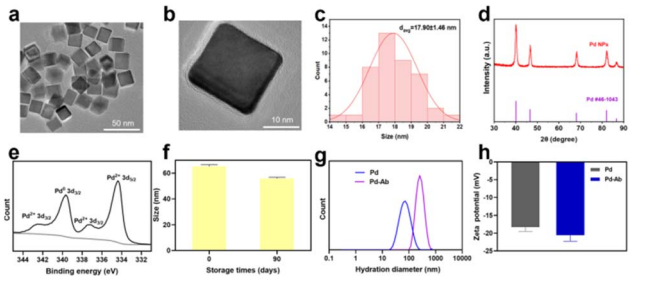

Fig. 1 Characterization of the PdNP morphology, structure and antibody conjugation. (a and b) TEM images of PdNPs; the scale bars are 50 nm (a) and 10 nm (b). (c) Histogram of the particle size distribution of PdNPs. (d) XRD pattern of PdNPs. (e) High-resolution XPS spectrum of Pd 3d. (f) Storage stability of PdNPs. (g and h) Hydration diameter and zeta potential of PdNPs before and after antibody conjugation.

diameter of PdNPs shifted from 72.5 nm to 254.4 nm after antibody conjugation, indicating successful binding (Fig. 1g). Additionally, the zeta potential of PdNPs shifted from −18.3 eV to 20.6 eV after antibody conjugation. Similarly, the zeta potential of the AuNPs shifted from −21.5 eV to 9.3 eV (Fig. S4†), further confirming successful conjugation of antibodies to nanoparticles (Fig. 1h). Conventional AuNPs typically rely on electrostatic adsorption (EA) for antibody conjugation,[12,35–39] whereas PdNPs utilized covalent chemical conjugation (CC) in this work. To evaluate whether CC is more suitable for PdNPs compared with EA, we compared the detection performance of PdNP strips functionalized with identical antibodies using both methods. Strips with CC demonstrated significantly enhanced detection efficiency compared to the EA method (Fig. S5†). In summary, these results demonstrate the successful synthesis of stable PdNPs, highlighting their potential applications as detection probes.

3.2 Optimization of strip conditions

To optimize the strip conditions for the best detection performance, we used an Lp-PLA2 antigen as the detection target to optimize the main factors affecting detection, including the amount of conjugated antibody, probe volume, sample volume, incubation time of probe and sample. An application called "Color Picker" was used to acquire the RGB value of T line (the darker the band, the lower the value). First, different amounts of antibodies (10 μg, 15 μg, 20 μg, 25 μg, and 30 μg) were conjugated with PdNPs to investigate the detection effects, and the test strips had a darker band and a lower RGB value of T line when 15 μg of antibody was conjugated, indicating a better detection effect (Fig. 2a). Subsequently, the probe volume incubated with the samples was optimized by exploring the detection effects with adding 5 μL, 7.5 μL, 10 μL, 12.5 μL, and 15 μL probes. The best detection performance was achieved when 12.5 μL detection probe was added (Fig. 2b). Similarly, the sample volume incubated with the detection probe was optimized when the detection probe was incubated with 40 μL, 50 μL, 60 μL, 70 μL, and 80 μL of the same concentration samples. Then, 50 μL sample volume led to a better detection effect (Fig. 2c). Finally, the incubation time of detection probe and sample was optimized for 5 min, 10 min, 15 min, 20 min, and 30 min, and an incubation time of 10 min was optimal for detection (Fig. 2d). Since the optimal detection conditions vary

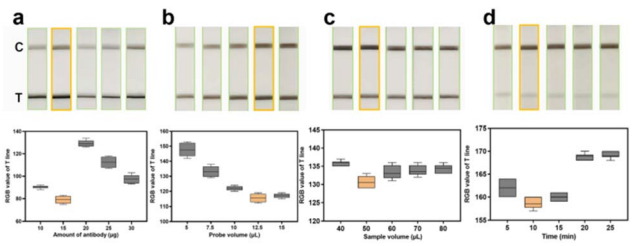

Fig. 2 Optimization of conditions for PdNP-based LFIA. (a–d) Detection results of test strips with different antibody concentrations, probe volumes, sample volumes, and incubation times between the sample and the probe.

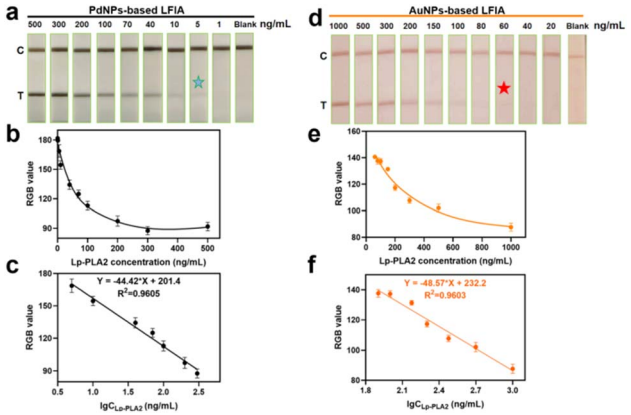

Fig. 3 Comparison of the analytical performance between PdNP-based LFIA and AuNP-based LFIA in Lp-PLA2 detection. (a and d) Representative photos taken of PdNP-based LFIA and AuNP-based LFIA. (b and c) Linear fitting between the signal intensity of T-line detected using PdNP-based LFIA and different target concentrations, as well as the corresponding linear relationships. (e and f) Linear fitting between the signal intensity of T-line detected using AuNP-based LFIA and different target concentrations, as well as the corresponding linear relationships.

for test strips based on different nanoparticles, we also optimized the same types of conditions affecting AuNP-based LFIA. The results indicated that for AuNP-based LFIA, an antibody conjugation amount of 15 μg, a probe volume of 10 μL, a sample volume of 50 μL, and an incubation time of 10 min resulted in better detection performance (Fig. S6†).

3.3 Performance comparison of PdNP and AuNP-based LFIA

The detection performance of PdNP and AuNP-based LFIA was compared under optimized conditions. A series of standard Lp-PLA2 at concentrations ranging from 0 to 1000 ng mL^{-1} were tested to evaluate two nanoparticle systems. As the target concentration increased, the T line color intensity gradually intensified. The visual limit of detection (vLOD) was defined as the minimum Lp-PLA2 concentration, at which the T line color intensity was significantly higher than the negative control. The results indicated that PdNP-based LFIA achieved a vLOD of 5 ng mL^{-1} for Lp-PLA2 (Fig. 3a), whereas AuNP-based LFIA exhibited a vLOD of 60 ng mL^{-1} (Fig. 3d), indicating a 12-fold lower

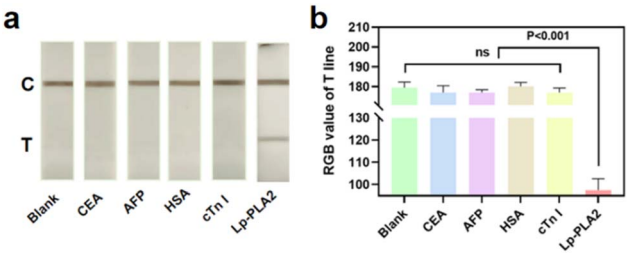

Fig. 4 Specificity results of the PdNP-based LFIA: (a and b) test strips for specificity experiment and quantitative results of the T-line signal intensity when detecting carcinoembryonic antigen (CEA), alpha-fetoprotein (AFP), human serum albumin (HSA), cardiac troponin I (cTn I), and blank (water).

Table 1 Recoveries of Lp-PLA2 spiked in serum samples[a]

	Spiked concentration (ng mL^{-1})	Mean ± SD (ng mL^{-1})	Recovery (%)	CV (%)
Lp-PLA2	40	41.79 ± 8.80	104.47	9.69
	70	68.76 ± 13.03	98.23	11.06
	100	107.20 ± 11.45	107.2	7.33

[a] SD: standard deviation; CV: coefficient of variation.

sensitivity for the PdNP system. The T line signal intensity showed a strong linear relationship with the logarithm of Lp-PLA2 concentrations over a 100-fold range (5–500 ng mL^{-1}) for PdNP strips (Fig. 3b and c). In contrast, the AuNP strips displayed a linear response only within a 16-fold narrower range (60–1000 ng mL^{-1}) (Fig. 3e and f). These findings highlight the superior performance of PdNP-based LFIA, which not only lowers the detection limit but also expands the quantifiable concentration range compared to the conventional AuNP-based LFIA.

3.4 Specificity and recoveries of PdNP-based LFIA

PdNP-based LFIA enhanced the sensitivity and broader dynamic range compared to AuNP-based LFIA, we further investigated the specificity of PdNP-based LFIA by testing a series group of disease biomarkers existing in human serum including carcinoembryonic antigen (CEA), alpha-fetoprotein (AFP), human serum albumin (HSA), cardiac troponin I (cTn I), Lp-PLA2 and water (blank). Strips tested with Lp-PLA2 exhibited a distinct T line, with the RGB value of T line showing statistically significant differences compared to other groups ($P < 0.001$). In contrast, no significant differences in RGB values of T line were observed among the non-target groups (Fig. 4a and b), confirming the high specificity of PdNP-based LFIA. To evaluate the quantitative accuracy of PdNP-based LFIA in complex biological matrices, recovery experiments were conducted using human serum spiked with standard Lp-PLA2 at concentrations of 40 ng mL^{-1}, 70 ng mL^{-1}, and 100 ng mL^{-1}. The T line RGB values obtained from these sample detected results were analyzed against the calibration curve to calculate the recovery rates. The measured recoveries were 104.47%, 98.23%, and 107.20% for the low-, medium-, and high-concentration groups, respectively (Table 1), all the results falling within the acceptable range of 90–110%. These results confirmed the robust quantitative capability of PdNP-based LFIA for detecting Lp-PLA2 in human serum.

3.5 Detection results of clinical samples

PdNP-based LFIA was further validated using 57 clinical serum samples. The detection process was illustrated in Fig. 5a, and the detected results were showed in Fig. 5b, the results showed the detected Lp-PLA2 concentrations were strongly in accordance with established clinical methods (Fig. 5c). The assay correctly distinguished positive and negative samples, and the ROC value was 0.98, demonstrating excellent specificity and sensitivity for the method (Fig. 5d and e). These findings underscore the high reliability and clinical utility of the PdNP-based LFIA, highlighting its potential for real-world diagnostic applications.

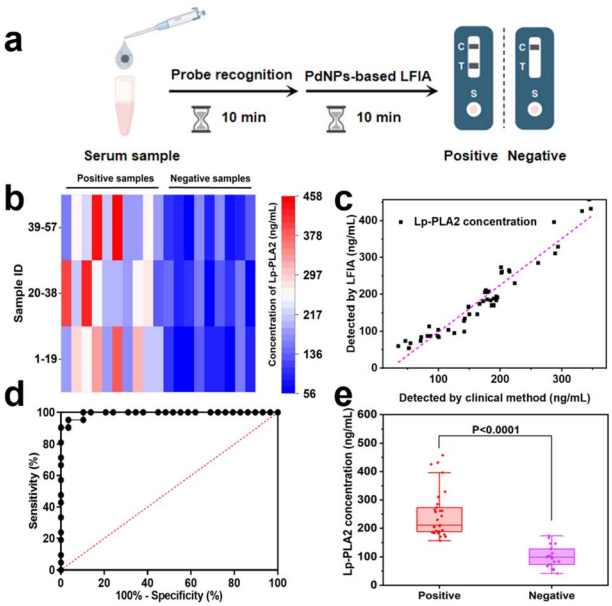

Fig. 5 Detection of Lp-PLA2 in serum of 57 patients using PdNP-based LFIA. (a) Procedure and time requirements for the detection of Lp-PLA2 in serum samples using PdNP-based LFIA. (b) Heat maps showing the results of Lp-PLA2 detection in clinical serum samples using PdNP-based LFIA. The value represented in the heat map is the concentration of Lp-PLA2 in each sample. (c) Comparison of the results for the detection of Lp-PLA2 in clinical serum samples using PdNP-based LFIA with clinical methods. (d) ROC curve for the detection of Lp-PLA2 in clinical serum samples using PdNP-based LFIA, with an area under the curve of 0.98. (e) Box plot result using PdNP-based LFIA to distinguish the positive and negative Lp-PLA2 clinical serum samples.

4. Conclusions

In summary, we synthesized stable PdNPs and designed PdNP-based LFIA, and the intrinsic black coloration of PdNPs provided a higher visual contrast at ultralow concentrations than AuNPs. Moreover, PdNP probes synthesized *via* chemical covalent conjugation with antibodies had the advantages of enhancing the target recognition ability. The synergy between covalent antibody conjugation and intrinsic black coloration addresses long-standing limitations in colorimetric signal detection. By comparing the detection performance under optimal conditions, we demonstrated that the PdNP-based LFIA

outperformed the traditional AuNP-based LFIA. The limit of detection of PdNP-based LFIA for Lp-PLA2 was 12-fold lower than that of AuNPs, and its linear concentration range was 100-fold wider, which far exceeded those of the AuNP-based LFIA. Furthermore, clinical validation confirmed the assay's practicality, with results correlating strongly with the established clinical methods. This work positions PdNPs as powerful alternatives to AuNPs in lateral flow diagnostics. While PdNPs demonstrated superior performance, their synthesis cost and long-term biocompatibility require further evaluation for large-scale clinical applications. Our future work will focus on multiplexed detection using PdNPs with tunable optical properties and integration with portable readout devices.

Data availability

Data are included within the article or ESI.†

Author contributions

Y. N., H. D. and Z. C. contributed equally to this work. Y. N.: conceptualization, methodology, software, formal analysis, investigation, data curation, and writing of the original draft. H. D. and Z. C.: methodology, formal analysis, investigation, and writing. W. Z.: methodology. J. C. and Z. L.: supervision and funding acquisition. Y. J. and M. C.: conceptualization, methodology, formal analysis, investigation, review and editing, and funding acquisition.

Conflicts of interest

The authors declare no conflict of interest.

Acknowledgements

This work was partially supported by the Fundamental Research Funds for the Central Universities (grant no. 2632024ZD07 and 2632024TD02).

References

1 A. Chen and S. Yang, *Biosens. Bioelectron.*, 2015, **71**, 230–242.
2 Z. Ma, J. Guo, L. Jiang and S. Zhao, *Talanta*, 2024, **267**, 125268.
3 V. G. Panferov, A. V. Zherdev and B. B. Dzantiev, *Biosensors*, 2023, **13**, 866.
4 S. Girotti, S. Ghini, E. Maiolini, L. Bolelli and E. N. Ferri, *Anal. Bioanal. Chem.*, 2013, **405**, 555–571.
5 C. Karakus and B. A. Salih, *J. Immunol. Methods*, 2013, **396**, 8–14.
6 X. G. Yang, Y. Wang, Y. Liu, J. F. Huang, Q. Q. Tan, X. Ying, Y. Hu and S. J. Li, *Front. Bioeng. Biotechnol.*, 2021, **9**, 758564.
7 Y. A. Akinshina, S. G. Mardanly, S. V. Rotanov, V. V. Pomazanov and V. A. Kiseleva, *Klin. Lab. Diagn.*, 2022, **67**, 91–96.
8 S. Kou, L. Liu, S. Song, H. Kuang, C. Xu and X. Wu, *Food Control*, 2024, **162**, 110402.
9 H. Deng, X. Cai, Y. Ji, D. Yan, F. Yang, S. Liu, Z. Deji, Y. Wang, Z. Bian, G. Tang, Z. Fan and Z. Huang, *Microchem. J.*, 2022, **179**, 107495.
10 H. Bao, M. Yuan, C. Xiao, D. Liu and W. Lai, *Food Chem.*, 2022, **375**, 131875.
11 C. Chen, B. Huang, W. Xu, R. Hou, B. Dong, X. Yu, Z. Wang and H. Li, *Sens. Actuators, B*, 2024, **412**, 135812.
12 D. Prakashan, N. S. Shrikrishna, M. Byakodi, K. Nagamani and S. Gandhi, *J. Med. Virol.*, 2023, **95**, e28416.
13 X. Xiao, S. Yu, G. Zhang, Z. Chen, H. Hu, X. Lai, D. Liu and W. Lai, *Small*, 2024, **20**, 7764.
14 H. Hu, J. Tian, R. Shu, H. Liu, S. Wang, X. Yin, J. Wang and D. Zhang, *Lab Chip*, 2024, **24**, 2272–2279.
15 M. Song, J. Xing, H. Cai, X. Gao, C. Li, C. Liu, X. Li, X. Fu, S. Ding, W. Cheng and R. Chen, *ACS Nano*, 2023, **17**, 10748–10759.
16 X. Tang, H. Zhang, J. Chen, D. Wu, Y. Wang, J. Sun, Z. Wang and X. Yang, *Anal. Chem.*, 2025, **97**, 2714–2723.
17 G. Zhang, S. Yu, J. Peng, Y. Xiong, L. Hu and W. Lai, *TrAC, Trends Anal. Chem.*, 2025, **183**, 118098.
18 M. Zhou, X. Chen, X.-a. Shen, X. Lin, P. Chen, Z. Qiao, X. Li, Y. Xiong and X. Huang, *J. Agric. Food Chem.*, 2023, **71**, 4408–4416.
19 X. Shao, X. Liu, L. Yu, X. Yu and J. Hu, *Microchim. Acta*, 2024, **191**, 733.
20 M. Mirasoli, A. Buragina, L. S. Dolci, M. Guardigli, P. Simoni, A. Montoya, E. Maiolini, S. Girotti and A. Roda, *Anal. Chim. Acta*, 2012, **721**, 167–172.
21 L. Wu, Z. Zhu, J. Xue, L. Zheng, H. Liu, H. Ouyang, Z. Fu and Y. He, *Biosens. Bioelectron.*, 2024, **265**, 116711.
22 M. Zangheri, L. Cevenini, L. Anfossi, C. Baggiani, P. Simoni, F. Di Nardo and A. Roda, *Biosens. Bioelectron.*, 2015, **64**, 63–68.
23 M. Zangheri, F. Di Nardo, D. Calabria, E. Marchegiani, L. Anfossi, M. Guardigli, M. Mirasoli, C. Baggiani and A. Roda, *Anal. Chim. Acta*, 2021, **1163**, 338515.
24 D. Calabria, M. M. Calabretta, M. Zangheri, E. Marchegiani, I. Trozzi, M. Guardigli, E. Michelini, F. Di Nardo, L. Anfossi, C. Baggiani and M. Mirasoli, *Sensors*, 2021, **21**, 3358.
25 S. Liu, C. Sun, X. Zhang, R. Shu, J. Zhang, B. Wang, K. Wang, L. Dou, L. Huang, Q. Yang and J. Wang, *Biosens. Bioelectron.*, 2025, **268**, 116920.
26 P. Tripathi, N. Upadhyay and S. Nara, *Crit. Rev. Food Sci. Nutr.*, 2018, **58**, 1715–1734.
27 J. Kim, M.-S. Shin, J. Shin, H.-M. Kim, X.-H. Pham, S.-m. Park, D.-E. Kim, Y. J. Kim and B.-H. Jun, *Int. J. Mol. Sci.*, 2023, **24**, 9600.
28 S. C. Razo, A. I. Elovenkova, I. V. Safenkova, N. V. Drenova, Y. A. Varitsev, A. V. Zherdev and B. B. Dzantiev, *Nanomaterials*, 2021, **11**, 3277.
29 L. Liao, M. Deng, Q. Gao, Q. Zhang, Y. Bian, Z. Wang, J. Li, W. Xu, C. Li, K. Wang, Z. Zheng, X. Zhou and G. Hou, *Int. J. Biol. Macromol.*, 2024, **275**, 837.
30 A. Onat and H. Direskeneli, *Curr. Pharm. Des.*, 2012, **18**, 1465–1477.
31 D. Li, W. Wei, X. Ran, J. Yu, H. Li, L. Zhao, H. Zeng, Y. Cao, Z. Zeng and Z. Wan, *Clin. Chim. Acta*, 2017, **471**, 38–45.

32 K. Adamiak and A. Sionkowska, *Int. J. Biol. Macromol.*, 2020, **161**, 550–560.
33 X. Meng, W. Zuo, P. Wu, Y. Song, G.-J. Yang, S. Zhang, J. Yang, X. Zou, W. Wei, D. Zhang, J. Dai and Y. Ju, *Nano Lett.*, 2023, **24**, 51–60.
34 M. Yuce and H. Kurt, *RSC Adv.*, 2017, **7**, 49386–49403.
35 Y. K. Chen, Z. Y. He, Y. X. Luo, Q. L. Su, Q. H. Wang, J. Z. Wang, J. K. He, M. L. Yu, H. You and H. L. Chen, *Spectrochim. Acta, Part A*, 2024, **320**, 124670.
36 H. Duan, L. R. Zhao, J. L. Wang, X. Wang, L. Y. Zheng and X. L. Huang, *Anal. Chim. Acta*, 2024, **1329**, 343233.
37 Z. Lai, F. Wang, Y. Cui, Z. Li and J. Lin, *Talanta*, 2025, **285**, 135812.
38 C. Parolo, A. de la Escosura-Muñiz and A. Merkoçi, *Biosens. Bioelectron.*, 2013, **40**, 412–416.
39 T. Y. You, Z. Y. Zhang, J. Y. Ma, Y. Jia, Y. Ding and X. D. Hua, *J. Food Compos. Anal.*, 2024, **134**, 106551.